GALAXIES IN DENSE CLUSTER ENVIRONMENTS

MS (Research) Thesis

By:
Sana Begum Murtuja Shaikh



DEPARTMENT OF ASTRONOMY , ASTROPHYSICS AND SPACE ENGINEERING

INDIAN INSTITUTE OF TECHNOLOGY INDORE

April, 2026

GALAXIES IN DENSE CLUSTER ENVIRONMENTS

A THESIS

Submitted in partial fulfillment of the requirements for the award of the degree
of
Master of Science

by
Sana Begum Murtuja Shaikh



DEPARTMENT OF ASTRONOMY , ASTROPHYSICS AND SPACE ENGINEERING

INDIAN INSTITUTE OF TECHNOLOGY INDORE

April, 2026

INDIAN INSTITUTE OF TECHNOLOGY INDORE

CANDIDATE'S DECLARATION

I hereby certify that the work which is being presented in the thesis entitled **Galaxies in dense cluster environments** in the partial fulfillment of the requirements for the award of the degree of MASTER OF SCIENCE (RESEARCH) and submitted in the DEPARTMENT OF ASTRONOMY, ASTROPHYSICS AND SPACE ENGINEERING, Indian Institute of Technology Indore, is an authentic record of my own work carried out during the time period from January 2024 to June 2025 under the supervision of Dr. Priyanka Singh assistant professor in IIT Indore. The matter presented in this thesis has not been submitted by me for the award of any other degree of this or any other institute.

Sana 02/04/26

Signature with date (Sana Begum Murtuja Shaikh)

This is to certify that the above statement made by the candidate is correct to the best of my knowledge.

Signature of the Supervisor of M.S(Research) Thesis
(Dr.Priyanka Singh)

Sana Begum Murtuja Shaikh has successfully given his M.S (Research) Oral Examination held on 1st April 2026

Signature(s) of Chairperson(OEB)

Date: 30/4/2026

Signature of Thesis Supervisor

Date:- 30/04/2026

Manoneeta Chakraborty

Signature of Convener,DPGC

Date:- 01/05/2026

S. Das

Signature of Head of Discipline

Date:- 04/05/2026

Acknowledgement

I would like to express my deepest gratitude toward my supervisor, Dr. Priyanka Singh, for her constant guidance and unwavering support. I am particularly grateful for her patience and willingness to explain complex concepts to me, often taking the time to sit down with pen and paper to ensure that I understood each aspect thoroughly. I want to extend my heartfelt gratitude towards my classmates Abhishek Darwai, Aman Dubey, Eeshaan Beohar, Rajat Katta, Ranjan Kumar, Tejas Rajuskar, and Sourodeep Hazra, as well as my labmates Abhinav Narayan, Samir Sethi and Thomas George, for their support and encouragement, keeping me motivated and inspired throughout my academic journey. Special Thanks to my best friend in IIT Indore, Shubhi Tiwari, for being there for me even in my difficult times; whenever I needed her, she was always there to support me emotionally and professionally. I thank my B.Tech friends Aarti, Aishwarya, Harvinder, Snehal, Sneha, Shivani, Vaishnavi, and Unnati for keeping me motivated throughout the journey. Thanks to my friend Irtesam, with whom I always used to discuss my highs and lows; thank you for listening to me throughout these two years of my journey. I am also thankful to my parents for having faith in me and allowing me to pursue my studies away from home, and also to my siblings Awej, Ayan, and Ishu for always being there for me. Additionally, I express my gratitude to IIT Indore and the Department of Astronomy, Astrophysics, and Space Science Engineering for providing me with the opportunity to pursue my academic and scientific interests in astronomy.

Some of the results in this paper have been derived using the 'healpy' and 'HEALPix' packages.

Abstract

Galaxy clusters represent some of the most extreme environments in the Universe. They are ideal locations to study the impact of an extreme environment on stellar evolution. In this work, we try to determine how the stellar mass function depends on factors such as the surrounding environments, whether they reside in isolated fields, galaxy groups, or clusters. We use the 9-band photometric galaxy data of the G9 patch from the Kilo Degree Survey (optical) and the VISTA Kilo-Degree Infrared Galaxy Survey (infrared), containing around 3.7 million galaxies, overlapping with the cluster catalog provided by the eROSITA Final Equatorial Depth Surveys (eFEDS). After applying appropriate selection criteria, we have 105 eFEDS clusters within the redshift range 0.385-0.8, covering ~ 46 square degrees. The large, continuous overlap of the surveys allows us to examine the SMF of the cluster galaxies within the cluster-centric radial bins up to $5R_{500}$. We find a clear detection of the cluster galaxy SMF up to $2R_{500}$ beyond which it's consistent with the background. We divide the cluster sample into redshift, mass, and luminosity bins to examine their impact on the SMF. The SMF of cluster galaxies for the high-mass clusters shows a decline at low stellar masses ($M_* \lesssim 2 \times 10^{10} M_\odot$) within $0 - 0.5R_{500}$, as compared to a flat SMF for the low-mass clusters, suggesting the low-mass galaxies grow over time before reaching the cluster center. Additionally, we find a higher SMF for the low redshift bin within $0.5R_{500}$ at stellar masses $M_* < 10^{10} M_\odot$. We also examined the effect of cluster ellipticity on the cluster galaxy SMF and found a higher SMF for low ellipticity clusters within $0.5R_{500}$, suggesting a link between the dynamical age and the stellar population growth in the cluster cores.

Contents

1 Introduction **1**
- 1.1 Galaxies in different environments . . . 1
- 1.2 Galaxy evolution . . . 2
- 1.3 Multi-wavelength studies of galaxies . . . 2

2 Review of Past Work and Problem Formulation **4**
- 2.1 Literature Review . . . 4
- 2.2 Problem Formulation . . . 5
  - 2.2.1 Caveats . . . 5
  - 2.2.2 Method . . . 5

3 Datasets **7**
- 3.1 KiDS+VIKING-450 (KV450) Galaxies . . . 7
- 3.2 eFEDS Clusters . . . 8
- 3.3 Cluster Galaxy Sample . . . 9
  - 3.3.1 Cluster galaxy selection process . . . 10

4 Sky coverage map for KV450 galaxies **12**
- 4.1 HEALPix . . . 12
- 4.2 Creating Map using healpy . . . 12
- 4.3 Calculation of Cluster Volume . . . 13

5 Stellar Mass Function (SMF) **14**
- 5.1 SMF For KV450 galaxies . . . 14
  - 5.1.1 Counting Galaxies in Stellar Mass Bins . . . 14
  - 5.1.2 Applying Stellar Mass Completeness Limit . . . 15
  - 5.1.3 Poisson Uncertainty . . . 15
- 5.2 SMF for Cluster Galaxies . . . 16
  - 5.2.1 Background/Foreground Subtraction . . . 18

6 Results and Discussions **21**
- 6.1 Redshift Dependence . . . 21
- 6.2 Cluster mass and luminosity dependence . . . 22
- 6.3 Dynamical State Dependence . . . 24

7 Conclusions and Scope for Future Work **27**
- 7.1 Conclusions . . . 27
- 7.2 Scope for future work . . . 28

References

List of Figures

3.1 Overlap of KV450 galaxies with eFEDS Field 9
3.2 total mass and redshift distribution of eFEDS clusters 10
3.3 Cluster galaxy sample. 11

4.1 KV450 Galaxy map 13

5.1 Mass completeness limit 15
5.2 Redshift vs Total Mass of Clusters 17
5.3 Footprint of G9 patch after masking the galaxies within the cluster radius $2R500$ 19
5.4 SMF for cluster galaxies within cluster-centric radial bins 20

6.1 Redshift, luminosity and mass dependent SMFs 23
6.2 Comparison of luminosity dependent SMF with the field galaxy SMF in two redshift bins (0.385,0.5) and (0.5,0.8) 24
6.3 Clusters' dynamical state dependent SMFs for the clusters with ellipticity(e) $e < 0.5$ and $e > 0.5$ 25
6.4 Clusters' dynamical state dependent SMFs for 10 highest and 10 lowest ellipticity clusters 25

Chapter 1

Introduction

Galaxies contain gas, dust, stars, and dark matter, bounded by their gravitational fields. Galaxies have various sizes and shapes, such as spiral, elliptical, and irregular. The stellar mass of a galaxy is the total mass of stars within it, dependent on the star formation rate of the galaxy, which represents the amount of new stellar mass created per unit of time, expressed as solar masses per year. Stars form from cold molecular hydrogen clouds of gas and dust in space, which start to collapse under their own gravity. As the cloud starts to collapse, it heats up and forms a protostar in its center. The protostar begins to gather more material from the surroundings due to its gravitational field. When the pressure and temperature of the protostar become high enough, the nuclear fusion reactions begin. The star formation of the galaxy depends on various factors such as the amount of cold molecular clouds present in the galaxy, which are called the stellar nurseries [32], dynamic processes going on inside the galaxy, like galactic winds[4][14], feedback processes[27], etc, and the surrounding environment of the galaxy. These factors cause growth or reduction in star formation over time.

1.1 Galaxies in different environments

Galaxies can be found in a completely isolated environment, small groups, and clusters. Field galaxies are the galaxies that evolve in isolation; they reside in low-density regions of the universe, and the halo mass for field galaxies is around $< 10^{12.5} M_{\odot}$. Galaxy groups are the small groups of galaxies containing very few to less than a hundred galaxies with halo mass range between $(10^{13} - 10^{14}) M_{\odot}$ while, galaxy clusters are the largest gravitationally bound structures that contain hundreds or thousands of galaxies held together with halo mass range $(10^{14} - 10^{15.5}) M_{\odot}$. Galaxies within the clusters have different environments compared to the isolated galaxies in the field, examples of the impact of a cluster environment are interactions with neighboring galaxies since clusters have higher densities of galaxies such as galaxy merger while merging their gas reservoirs get compressed cause the starburst in high density regions only for a short time and then eventually cause reduction in star formation[3][17], tidal forces from clusters gravitational potential can strip away cold gas of galaxies from its outer layer [23][8], ram pressure stripping due to the presence of hot ($T \sim 10^7 - 10^8 K$) intracluster medium (ICM), which exert pressure on the galaxy moving through it and strips away the cold gas from the galaxy disk[13][15], etc., results in low star formation rate or even halt the star formation which affects their evolution over a cosmic time, while field galaxies which reside in less dense and isolated regions undergo fewer interactions with neighboring galaxies compared

to cluster galaxies. Field galaxies undergo internal quenching (reduction or complete shutdown of star formation) processes, such as stellar and supernova feedback, AGN feedback, and gas exhaustion. The energy released from the massive stars or supernova bursts causes the outflow or heating of cold gas in the interstellar medium. And over time, the galaxy uses all its gas reservoirs for the ongoing star formation and eventually causes quenching due to the unavailability of cold gas, etc.

1.2 Galaxy evolution

Along with galaxy environments, galaxy redshifts are also critical while looking into how galaxies have evolved through cosmic time. Redshifts are used to track how galaxies change over time and help us understand how they form, grow, and evolve over billions of years. Typically, redshift is computed by spectroscopic and photometric means. Photometric redshifts are calculated by measuring galaxies' brightness in a range of wavelength bands known as photometry. On the other hand, spectrometric redshifts are calculated by analyzing the spectrum that the galaxies release and measuring the shift in the spectrum, called spectroscopy. Kim et al.(2023)[16] studied 1,626 galaxies with spectroscopic observations in 105 galaxy clusters in the redshift bin (0.26, 1.13) to quantify how the cluster environment affects the star formation of their galaxies. They found that the longer the galaxy stays in the cluster, the older its stellar population becomes, suggesting the slowdown of star formation due to the cluster environment, irrespective of the redshifts and galaxy luminosities. However, such spectroscopic studies are limited by small galaxy samples. Spectroscopy provides detailed information about the object, such as its composition, velocity using the Doppler shift in its spectra, temperature, and better object classification. It gives a more accurate measurement of redshifts compared to photometry. But spectrometry consumes more time to analyze the spectra of a large number of objects, so these surveys generally have a limited field of view, and the spectrometers are more expensive and complex to operate than the photometers. While photometry can be used for large surveys as they are cost-effective and less time-consuming, we can determine most of the properties of objects due to multi-band observations.

1.3 Multi-wavelength studies of galaxies

Astronomical surveys play an important role in understanding galaxies at different wavelengths. These surveys are conducted to study the large-scale structures in the universe. These surveys aim to observe a significant portion of the sky in specific wavelength bands with a specific survey goal and are carried out with telescopes having sensitive cameras and detectors that can detect the light coming from a source in different wavelength bands. Then the calibrated images are used for flux measurements in different wavelength bands. Flux refers to the amount of light received from an object, which allows quantifying the brightness of the object received by the sensor or detector. These surveys provide the catalogs based on their observations, such as providing the data about positions, redshifts, luminosity, magnitudes, etc., of the detected sources, and enable the mapping of large-scale structures in the universe, such as galaxies, galaxy clusters, and many more. The sky surveys, which are based on photometry, are called photometric surveys. Some examples of photometric surveys are the Dark Energy Survey (DES)

[2], the Two Micron All Sky Survey (2MASS) [28], the COSMOS/UltraVISTA Survey [25], etc. Photometric surveys made galaxy evolution studies easier by providing data on galaxy distribution over large sky regions and the measurements of their properties. While X-ray observations carried out with telescopes like Chandra, XMM-Newton, eROSITA, etc., are powerful for detecting galaxy clusters with the observation of hot intracluster gas, which indicates massive, gravitationally bound systems. The union of these two data sets enables robust characterization of cluster membership and makes possible the examination of how processes on cluster scales affect galaxy properties and their evolutionary paths.

To understand how galaxies evolve as they enter dense cluster environments, it is crucial to compare the environments of galaxies in the isolated field with those inside clusters (or inside a cluster within various radial bins) to analyze the cluster center and the cluster outskirts. One of the important aspects to study about galaxy environments is their stellar mass functions (SMFs), which show how the number density of galaxies changes with respect to their stellar masses. Comparing the SMFs of galaxies in various environments and at various redshift ranges enables us to reveal important insights into the process that molds galaxies' evolution.

Chapter 2

Review of Past Work and Problem Formulation

2.1 Literature Review

Several observational studies have tried to explain the impact of the environment on the stellar mass function of galaxies. Eg, Van der Burg (2013)[30] studied 10 clusters from the GCLASS survey and compared the SMF of cluster galaxies with the field at $z \sim 1$ using the 11-band photometry galaxy data from the COSMOS/UltraVISTA survey. They divide the galaxies further into star-forming and non-star-forming (quiescent) galaxies using their U-V and V-J colors. They found that at lower stellar masses, the total SMF (including all the galaxies) has a decline for the field galaxies compared to the cluster galaxies, but in the comparison of field vs cluster galaxies for the quiescent as well as star-forming galaxies, have no significant difference.

Tomczak et al. (2017)[29] studied how the local environment affects the evolution of galaxies by studying the SMFs of galaxies from the galaxy data (containing field and cluster galaxies) drawn from the ORELSE survey within $0.55 < z < 1.3$. They derived the stellar masses from SED fitting using the code FAST[19]. They also used galaxy divisions as star-forming and quiescent. Their results show that the shape of SMF varies according to the environment; the denser regions have a higher proportion of massive galaxies as compared to low-density regions. The SMF for star-forming galaxies doesn't vary much across the environments, but the massive quiescent galaxies are more in the denser regions.
Van der Burg et al. (2018) [31] studied 21 most massive clusters identified through the Planck SZ survey with multi-band photometry ranging from u ($\sim 3000A^{\circ}$) to Ks ($\sim 22000A^{\circ}$) band with the redshift range 0.5 to 0.7. They aimed to understand the environment's impact on galaxies' behavior as they move towards the cluster center. To achieve this, they compared the SMF of galaxies within cluster environments to that of galaxies in the field at similar redshift ranges, using the COSMOS/UltraVISTA survey's dataset. In addition to this, they categorized the galaxies as star-forming and passive galaxies using their rest frame U-V and V-J colors, and also compared the SMF of Star-forming and passive galaxies for field vs cluster galaxies at a given redshift range. They calculated the stellar masses for each galaxy and constructed a catalog from the UltraVISTA main catalog, only using 8 filters uBVrizJKs for each cluster. They calculated the photometric redshift for the galaxies using the posterior probability distribution

function given by the template fitting code EAZY[5] and also calculated a δz scatter to compare spectroscopic versus photometric redshifts. where $\Delta z = (z_{\rm ph} - z_{\rm spec})/(1 + z_{\rm spec})$. They calculated the SMFs for star-forming and quenched galaxies for field and cluster galaxies and a total SMF for all galaxies. The SMF comparison of the field to cluster galaxy showed that there is a higher quenched fraction of galaxies in the cluster as compared to the field making low mass slope steeper in cluster SMF but the shape of star-forming galaxies is the same showing that it is independent of the environment and the total SMF including both galaxies didn't vary significantly. They compared the cluster SMF in four radial bins starting from the cluster center to $2R_{500}$, each differing by the cluster radius of $0.5R_{500}$. They found that the quenching fraction of low mass galaxies is nearer to the center and decreases as we move away from the center due to the environment quenching which cause the decrease in quiescent galaxy SMF at lower stellar masses but there is no significant change in SMF shape for quenched galaxies and also no significant shape changes in total SMF between the radial bins.

2.2 Problem Formulation

2.2.1 Caveats

The main caveats of these works, which cause the biases in the field to cluster galaxy SMF comparisons, are:

1. **Limited data set:** these studies contain a limited sky coverage of their multi-wavelength galaxy sample. Due to the small sky coverage, cosmic variance plays a crucial role. Cosmic variance refers to the statistical fluctuations or variations in observations of cosmic structures in a small sample area, as the universe is not perfectly homogeneous.

2. Use of different multi-wavelength surveys for field versus cluster galaxy samples.

3. This survey analyzed the cluster samples up to a small range of cluster-centric radii, not analyzing the cluster outskirts properly. While comparing the cluster SMF with the field SMF.

To address these caveats, we used the combined nine-band photometric data of the Kilo Degree Survey (KiDS)[20] and the VISTA Kilo Degree Infrared Galaxy Survey (VIKING)[10] with a common $\sim$341 deg^2 survey area, jointly referred as KiDS+VIKING-450(KV450)[35]. Both of these surveys were conducted by the European Southern Observatory (ESO) and 105 eROSITA Final Equatorial-Depth Survey (eFEDS)[21] clusters, which are a part of the eROSITA All Sky Survey(eRASS)[7]. From the survey overlap, we calculated the SMF for cluster galaxies and their coeval fields, and compared these two. In addition to this, we compared the SMF of the cluster within the cluster-centric radial bins to study the environmental effects within the clusters. We analyzed the cluster outskirts up to $5 \times R_{500}$, thanks to the continuous coverage of the photometric surveys under consideration.

2.2.2 Method

Below is a summary of the steps involved in our analysis.

1. First, we verify the SMFs of KV450 galaxies at different redshift bins using the $1/V_{\max}$ method with added Poisson uncertainty. Our results are consistent with those provided by Wright et al. (2019)[35]

2. For the cluster galaxy sample, we have assigned the galaxies to the cluster that are within the cluster-centric radial bins and have an uncertainty in redshift range $z \pm \Delta z$ where z is the cluster redshift. We have calculated the R_{500} and Δz.

3. For the cluster membership, we have assigned the galaxies to the cluster that are within the cluster-centric radial bins(multiples of R_{500}) and having an uncertainty in redshift range $z \pm \Delta z$ where z is the cluster redshift. We have calculated the Δz uncertainty in cluster galaxy redshift.

4. We applied a selection criterion on the KiDS+VIKING-450 dataset, which causes the reduction of galaxies, leaving some of the clusters with empty patches. To overcome this bias, we created a HEALPix map for field galaxies and calculated the cluster area and volume using the non-zero galaxy pixels.

5. For cluster galaxy SMF, we started by calculating the number of galaxies within the cluster-centric radial bins at a given redshift bin, and removed all the galaxies below the stellar mass completeness limit. Then we computed the SMF by counting the galaxies within the stellar mass bins. We introduced the Poisson uncertainty to SMF data points, which is the square root of the galaxy count within stellar mass bins, by propagating the error.

6. To ensure there is no influence of field galaxies on cluster galaxy SMF, we removed their coeval field SMF of the clusters from the calculated SMFs. We considered the radial bin $4 - 5R500$ as a field. To calculate this field SMF, we masked the clusters up to $2R_{500}$

7. We divided the clusters with respect to their median redshift, median mass, and median luminosity, calculated the cluster galaxy SMF within different radial bins, and then compared them within the same redshift range. to quantify the effect of mass and luminosity on the cluster galaxy SMF.

8. To quantify the effect of clusters' dynamic nature on galaxy evolution, we chose 20 clusters, 10 with the lowest and 10 with the highest ellipticity from the 105 clusters, and compared their SMFs.

Chapter 3

Datasets

To study the impact of the galaxy cluster environment on the SMF of the galaxies residing in the field compared to cluster galaxies, for the galaxy properties such as stellar masses and photometric redshifts, we are using the KiDS+VIKING-450 dataset publicly available by Wright et al. 2019 [35], along with data from the eROSITA Final Equatorial-Depth Survey (eFEDS)[21] for the clusters.

3.1 KiDS+VIKING-450 (KV450) Galaxies

The KiDS (Kilo Degree Survey)[20] and VIKING (VISTA Kilo degree Infrared Galaxy)[10] surveys were jointly designed to provide well-aligned optical and near-infrared (NIR) data across ∼1350 deg^2 of the sky in both the Galactic North and Galactic South regions. The surveys were planned to have nearly identical coverage areas in the sky. Both surveys have already completed their imaging over the planned sky area, VIKING with DR4 in February 2020 and KiDS with DR5 in June 2024 [36]. The KiDS-450 dataset after masking is divided into five distinct patches on the sky shown in figure 4.1 named as G15, G12, G9, GS, and G23, primarily centered on fields observed by the the Galaxy And Mass Assembly (GAMA) redshift survey [9] except GS patch.

Wright et al. (2019) [35] combined optical ugri-band ((3000-9000 Å)) data from the KiDS survey and near-infrared ZYJHKs-band (8000-24000 Å) data from the VIKING survey. The combined KV450 sample is defined as only those KiDS-450 sources that overlap with VIKING imaging and masked all other sources with missing near infra-red coverage. This combination of survey depth ($r \leq 25$) where r is magnitude in r-band and the use of a nine-band wavelength coverage (ugriZYJHKs) enables substantial reductions in systematic uncertainties, including outlier rates and scatter, when comparing photometric and spectroscopic redshifts. KV450 covers ∼341 deg^2 with 447 overlapping pointings. It includes around 31.9 million primarily extragalactic sources. The authors have provided photometry, photo-z estimates, and stellar masses for the sources.

The catalog presented by Wright et al. (2019) [35] consists of ∼ 49 million all extragalactic sources, including stars and galaxies. We have applied a selection criteria for galaxies ($mask \leq 4$) on the dataset, removed all the stars, and also removed all galaxies for which the stellar masses were undetermined, after the reduction, the data set is reduced from ∼ 49 million extragalactic sources to ∼ 31 million galaxies and then this reduced KV450 catalog is used for further calculations.

3.2 eFEDS Clusters

The eROSITA Final Equatorial-Depth Survey was conducted during the evaluation verification stage of the eROSITA X-ray telescope, in the first quarter of November 2019. Spanning ∼140 deg^2 ($126° < \mathrm{RA} < 146°$ and $-3° < \mathrm{Dec} < +6°$) of the sky, the eFEDS survey has identified 542 potential candidates of clusters and groups of galaxies through X-ray selection. These clusters are spread out across a range of redshifts, from 0.01 to 1.3, having a median redshift at 0.35. Several observations have been conducted on the eFEDS field using various survey instruments across different wavelength bands, ranging from optical to radio. These observations include confirmation, estimating weak-lensing masses, and determining redshifts for eFEDS clusters.

Liu et al. (2022)[21] presented the catalog of groups and galaxy clusters identified within the eFEDS field with a likelihood extent defined as $L_{\mathrm{ext}} = -\ln(P)$ where P is probability that the detected source is consistent with a point-source model. In their analysis a threshold of $L_{\mathrm{ext}} > 6$, results in an estimated purity of approximately 80% for the entire cluster sample. Their study also included the inaugural results of an X-ray analysis for these galaxy groups and clusters based on the data from eROSITA. They used the multicomponent matched filter (MCMF) tool to compute photometric redshifts for the clusters by analyzing the photometric dataset from DECaLS, unWISE, and HSC surveys. The photometric redshift distribution of these clusters is shown in Figure 3.2(b). Spectroscopic redshifts were derived through cross-matching with various publicly available spectroscopic surveys, such as 2MRS, SDSS up to DR16, and GAMA. They provided spectroscopic redshifts for a total of 297 clusters.

Klein et al. (2022) [18] performed the optical follow-up of the eFEDS 542 group and cluster candidates to provide their redshift, dynamical state, richness, masses, etc. The mass distributions of these clusters are shown in Figure 3.2(a), respectively.

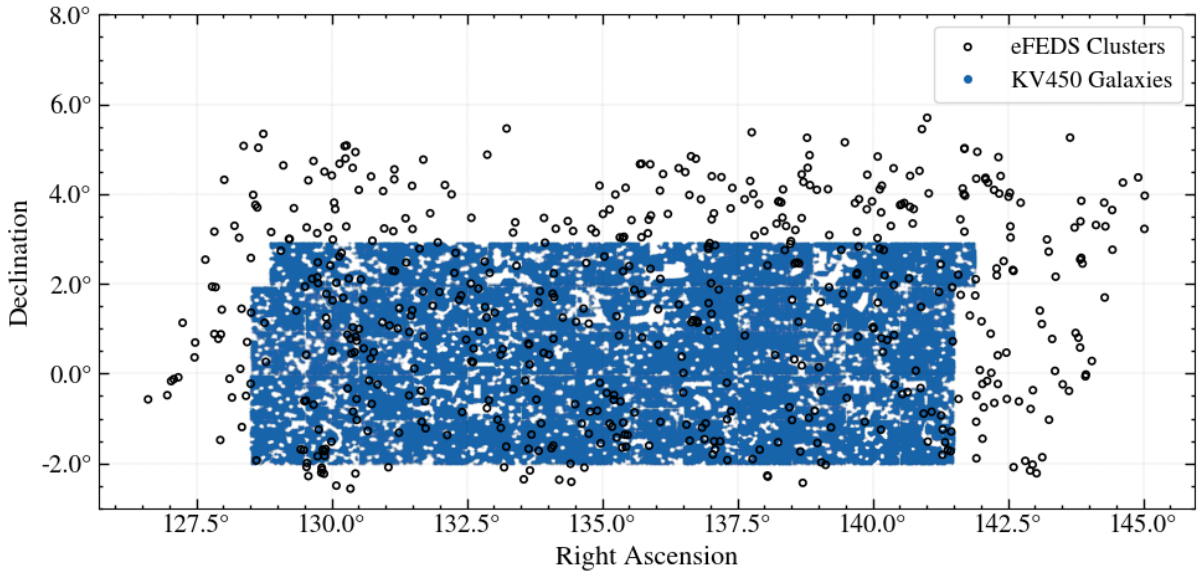


Figure 3.1: Footprint of eFEDS Field having a overlap with KV450 galaxies. The blue-colored region shows the overlapping of KV450 (G9) patch galaxies with eFEDS clusters, and cluster positions are shown with black circles.

3.3 Cluster Galaxy Sample

The eFEDS field overlaps with the G9 patch of KV450 shown in Figure 3.1. From the overlap, we have created cluster galaxy samples. We used the cluster galaxy data, such as the galaxies which belong to the eFEDS clusters if they are within the cluster radius (R_{500}) and redshift uncertainty ($\pm\Delta z$), while z is the cluster redshift. We assigned the KV450 galaxies to the eFEDS clusters, which should be part of a specific cluster at a given cluster redshift and cluster-centric radial bin.

The cluster radius is measured in (R_{500}), where the mean density of the cluster is 500 times the universe's critical density. Klein et al. (2022)[18] provided the mass of clusters M_{500} (refer Figure 3.2(a)) and calculated the luminosity - mass (L-M) scaling relationship from Bulbul et al. (2019)[6] given by,

$$L_{500,\,0.5-2.0} = A_X \left(\frac{M_{500}}{M_{\rm piv}}\right)^{B_X} \left(\frac{E(z)}{E(z_{\rm piv})}\right)^{2} \left(\frac{1+z}{1+z_{\rm piv}}\right)^{\gamma_X} \tag{3.1}$$

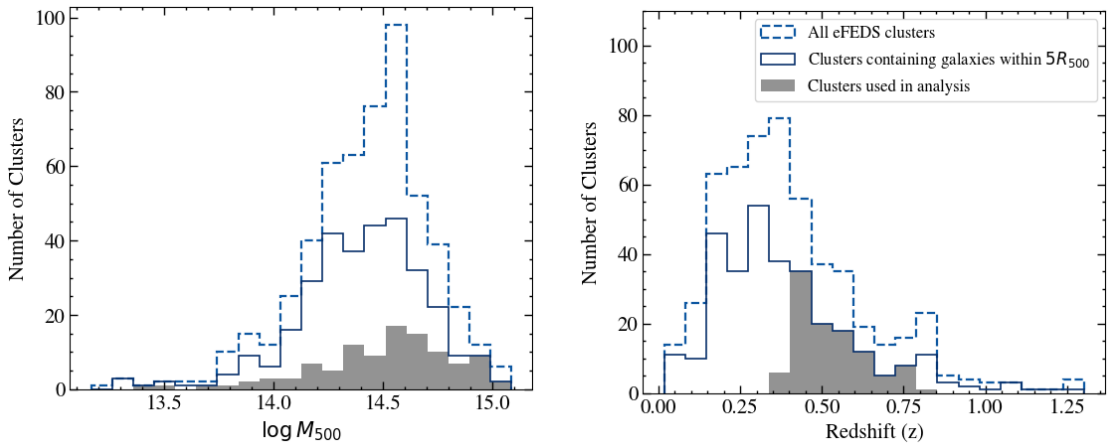
Where $L_{500,\,0.5-2.0}$ is luminosity calculated in the energy range 0.5-2.0 keV within R_{500},$E(z)$ is the dimensionless Hubble parameter. For this scaling relation the best-fit parameters are

$A_X = 4.15 \times 10^{44}$ erg s^{-1}, $B_X = 1.91$, and $\gamma_X = 0.252$. The pivot mass and redshift are $M_{\rm piv} = 6.35 \times 10^{14}\ M_\odot$ and $z_{\rm piv} = 0.45$, respectively.

We have Calculated R_{500} for the given M_{500} of a cluster by using the following formula,

$$M_{500} \equiv 500 \left(\frac{4\pi}{3}\right) R_{500}^3 \times \rho_c \tag{3.2}$$

$$R_{500} \equiv \left(\frac{3 \times M_{500}}{500 \times 4\pi \times \rho_c}\right)^{\frac{1}{3}} \tag{3.3}$$



(a) Total mass distribution

(b) photometric redshifts Distribution

Figure 3.2: Total mass and redshift distribution of eFEDS clusters. The dashed line shows all 542 clusters, the solid line represents the total 313 clusters that have KV450 galaxy coverage within $5R_{500}$, and the grey-shaded region shows the final sample of 105 clusters used in SMF analysis within the redshift range (0.385, 0.8).

Where ρ_c is the critical density of the Universe, the required average density of matter to halt the universe's expansion. For each cluster, we have calculated ρ_c, which is a function of redshifts using astropy. The angular sizes (corresponding to R_{500}) of these clusters are,

$$\theta_{500} = \left(\frac{R_{500}}{D_A}\right) \tag{3.4}$$

D_A is the angular diameter distance of the cluster, dependent on redshift.

3.3.1 Cluster galaxy selection process

To identify galaxies that should be cluster members, we use the photometric redshift uncertainties of galaxies. Wright et al. (2019) [35] calculated photometric redshifts from 9-band (ugriZYJHKs) photometry for the KV450 using Bayesian Photometric Redshifts (BPZ), a large number of spectroscopic redshift samples from different surveys are used. They compare spectroscopic redshifts($z_{\rm spec}$) to photometric redshifts($z_{\rm ph}$) using the following formula;

$$\frac{z_{\rm ph} - z_{\rm spec}}{1 + z_{\rm spec}} \equiv \frac{\Delta z}{1 + z} \tag{3.5}$$

Where, $\Delta z/(1+z) = \sigma_m$. σ_m is the median absolute deviation. The calculated values for σ_m are 0.061 for $z_{\rm ph} \leq 0.9$ and 0.096 for $z_{\rm ph} > 0.9$. We have used the same σ_m to calculate the redshift uncertainty for cluster galaxies, where $\Delta z = (1+z) \times \sigma_m$, z is the cluster redshift, and $\pm\Delta z$ is its uncertainty. Figure 3.3 shows one of the cluster galaxy samples from our cluster galaxy data.

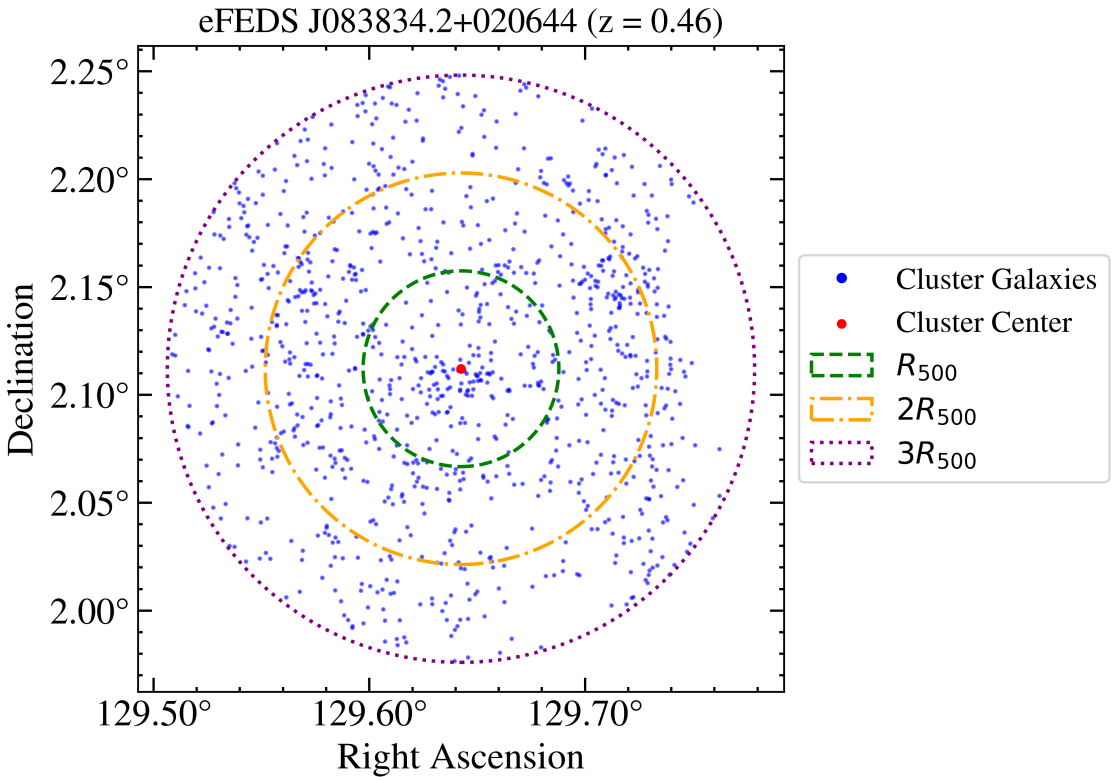


Figure 3.3: Shows the cluster named eFEDS J083834.2+020644 at redshift, $z = 0.46$ with the cluster centric radii R_{500}, $2R_{500}$ and $3R_{500}$ shown in green, orange and purple color respectively, with R_{500}= 0.95Mpc. Galaxies within the cluster centric radii are shown in blue color with redshift range $z \pm \Delta z$, $\Delta z = 0.089$, and the red dot is the cluster center. As we move away from the cluster center, the number of galaxies per volume decreases. The cluster has 181 galaxies within R_{500}, 427 galaxies within 1-2R_{500} and 452 galaxies within 2-3R_{500}

Chapter 4

Sky coverage map for KV450 galaxies

We have created a sky coverage map for the KV450 galaxy dataset with the aim of calculating the cluster volume within the cluster-centric radial bins using HEALPix[1] pixelization scheme as described below.

4.1 HEALPix

HEALPix stands for Hierarchical Equal Area isoLatitude Pixelization. This pixelization scheme is commonly used to map the celestial sphere onto a grid of pixels[11]. It divides the celestial sphere into several pixels with the same area, such that each pixel covers the same solid angle on the sky.

4.2 Creating Map using healpy

'healpy' is a Python package designed to handle pixelated data on a sphere based on the HEALPix scheme. It provides a number of functions and tools to create and manipulate HEALPix maps[37].

N_{side} is a parameter that defines the resolution of the HEALPix map. it specifies the number of divisions along each axis of a HEALPix grid. The value of N_{side} should be 2^k where k=0,1,2,3,....n, and n is a positive integer. the total number of pixels in a HEALPix map is $12 \times {N_{side}}^2$ it means the HEALPix grid is initially divided with 12 equal area pixels at k=0 and each time we increase the value of k by 1 each pixel get divided into further 4 new pixels with equal area. The higher values of N_{side} correspond to smaller pixel areas and higher resolutions.

We used a large N_{side} equal to 4096, where k=12, which corresponds to a pixel resolution equal to $\approx$ 51.5 arcseconds. With this resolution, we obtain a mean of 16 galaxies per pixel calculated for the pixels with at least one galaxy. To further avoid shot noise due to the low number of galaxies per pixel or not to overestimate the cluster volumes, we considered only the pixels that contain at least five galaxies. The calculated area for KV450 with this resolution is ~ 379.67 deg^2, and the final area for the G9 patch is ~ 46 deg^2. The areas are calculated after applying the selection criteria on the galaxy dataset mentioned in the section 3.1.

4.3 Calculation of Cluster Volume

As we applied several selection criteria or masking on the KV450 data set, we started to lose some of the coverage areas within the clusters. Additionally, the clusters near the survey boundary are not evenly covered. To overcome this, we normalize the cluster SMF by dividing it by the total usable volume of clusters. We calculate the cluster area using the HEALPix KV450 map by only considering pixels where at least 5 galaxies are present, we multiply the total number of such pixels within the given radial bin by the single pixel area of the map to compute the total area of a cluster within that bin. The calculated area was in degrees sq., so we converted it to Mpc sq., such that the total cluster area containing galaxies in the radial bin equals the fraction of pixels with at least 5 galaxies to all pixels within the given radial bin times the area of the radial bin. Then we estimated volumes for cluster radial bins. We considered the projection of the cluster over the sky as a cylinder with height as comoving length associated with $2\Delta z$ as $\pm\Delta z$ is the cluster galaxy uncertainty. The cluster Volume $V^c_{j,i}$ is given as:

$$V^c_{j,i} = A^c_{j,i} \times \left[D_c(z + \Delta z) - D_c(z - \Delta z)\right] \tag{4.1}$$

where $V^c_{j,i}$, $A^c_{j,i}$ are the volumes and areas of the i^{th} radial bin and j^{th} cluster respectively, and D_c is the comoving distance.

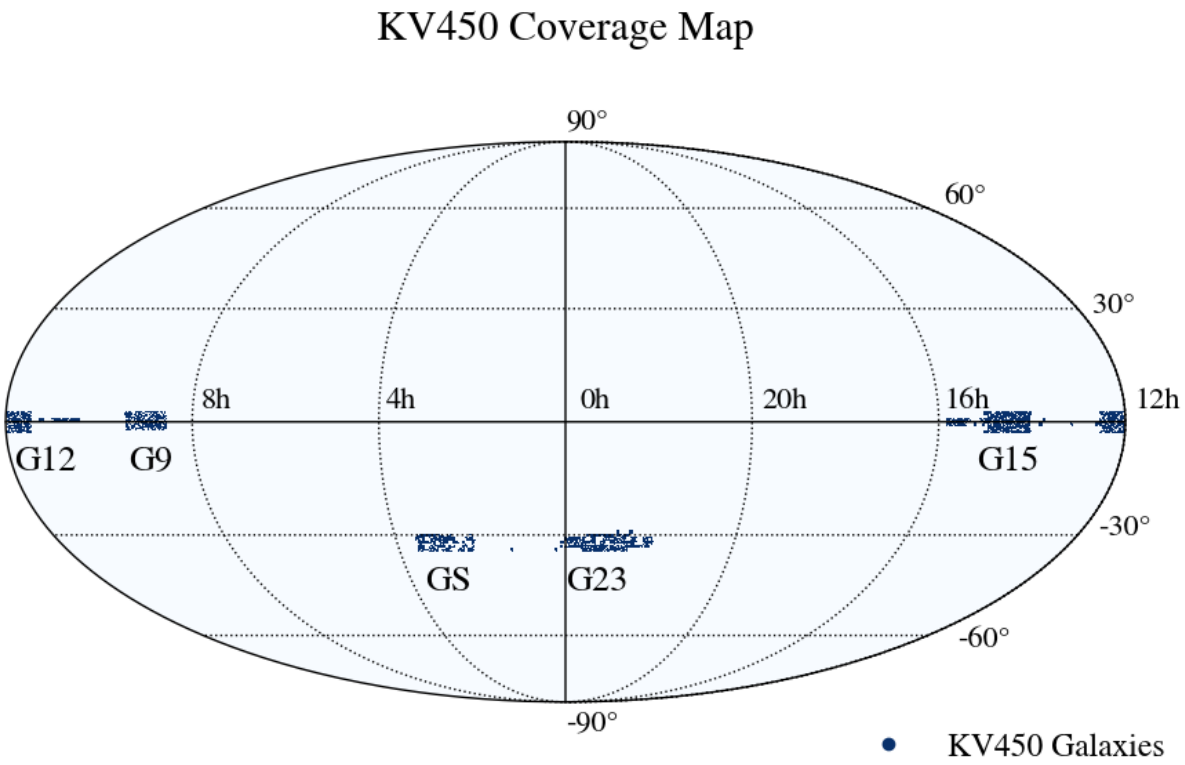


Figure 4.1: HEALpix map showing the KV450 galaxies distributed in five patches over the sky with the resolution of 51.5 arcsec.

Chapter 5

Stellar Mass Function (SMF)

5.1 SMF For KV450 galaxies

The stellar mass function (SMF) is a statistical distribution that describes the number density of galaxies as a function of their stellar masses. We have calculated and verified the SMF for the KV450 galaxies within different redshift bins; the steps involved are explained below.

5.1.1 Counting Galaxies in Stellar Mass Bins

First, we started calculating SMF by counting the galaxies within the bins of their stellar masses. We used the stellar mass bin width of 0.25 dex. Then we have applied the $1/V_{\rm max}$ given by Schmidt (1968) [26][33] where $V_{\rm max}$ is a maximum comoving volume which is a function of redshift, comoving volume is the amount of space occupied by the galaxy while the universe's expansion over time is taken into account.

Intrinsically faint galaxies are less likely to be detected by the selection criteria of the survey compared to the brighter sources, which is called the Malmquist bias. This bias particularly affects NIR samples where faint galaxies may have low luminosities and masses and can only be detected at lower redshifts within a limited volume of space. The $1/V_{\rm max}$ Method corrects this bias by figuring out the largest possible volume where each detected object can be seen. The maximum observable comoving volume ($V_{{\rm max},j}$) for the j^{th} galaxy within the redshift bin $z_{\rm low} < z < z_{\rm high}$ is given by:

$$V_{{\rm max},j} = \frac{4\pi}{3} \times \frac{\Omega}{\Omega_{\rm sky}} \times \left(D_{\rm c}(\min(z_{{\rm max},j}, z_{\rm high}))^3 - D_{\rm c}(\max(z_{{\rm min},j}, z_{\rm low}))^3 \right) \tag{5.1}$$

where Ω represents the sample's projected solid angle on the sky, and $\Omega_{\rm sky}$ is defined as 41253 deg^2, representing the solid angle of the celestial sphere. $D_{\rm c}(z)$ denotes the comoving distance at redshift z. Additionally, $z_{\rm max}$ stands for the maximum redshift at which the best fit spectral energy distribution (SED) of a galaxy can be no longer observable due to the flux limit of the survey, while $z_{\rm min}$ corresponds where the source's brightness could potentially exceed the camera's capacity and saturate it. In practice, $z_{\rm low}$ represents the lower boundary of the redshift bin within which the j^{th} galaxy lies.

The SMF of KV450 galaxies within i^{th} stellar mass bin calculated using $1/V_{\rm max}$ method

for a given redshift bin is given as

$$\phi_i(M_*) = \frac{1}{\Delta \log M_*} \times \sum_j \frac{1}{V_{\max,j}} \tag{5.2}$$

Note that we kept the stellar mass bin width, which is $\Delta \log M_* = 0.25$ dex throughout the analysis.

5.1.2 Applying Stellar Mass Completeness Limit

After calculating the galaxies within the mass bins and the given redshift bin, we applied mass completeness by removing all the galaxies below the mass completeness at the upper redshift limit of the calculated SMF. The mass completeness limit is the minimum stellar mass that a galaxy can have at a specific redshift to be detected by the surveys. Galaxies with stellar masses below this limit are too faint to be detected accurately by the survey instruments, and many of them get missed, causing incompleteness while analyzing galaxy samples. We used the stellar mass completeness limit from Wright et al. (2019) [35] calculated as flux scale-corrected stellar masses using the LE PHARE template fitting code, the mass completeness limits for KV450 galaxies are shown in Figure 5.1.

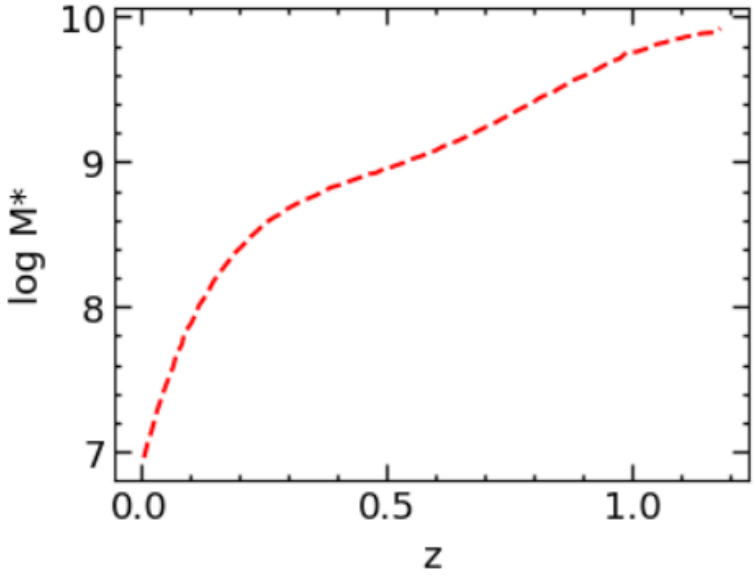


Figure 5.1: Mass completeness limit of KV450 galaxy stellar masses as a function of their redshifts

5.1.3 Poisson Uncertainty

Poisson noise arises when we start counting the galaxies within the stellar mass bins, which is a discrete quantity. To quantify this uncertainty, we calculated the Poisson error as $\sigma_N = \sqrt{N_i^g}$, where N_i^g represents the count of galaxies within the i^{th} stellar mass bin.

Using the propagation of error, we calculated the Poisson uncertainty as given below.

$$\phi_i(M_*) = \frac{1}{\Delta \log M_*} \times \sum_j \frac{1}{V_{\max,j}}$$

From the relation,

$$\left\langle \frac{1}{V_{\max,j}} \right\rangle = \frac{1}{N_i^g} \sum_j \frac{1}{V_{\max,j}} \tag{5.3}$$

equation 5.3 becomes,

$$\phi_i(M_*) = \frac{N_i^g}{\Delta \log M_*} \left\langle \frac{1}{V_{\max,j}} \right\rangle \tag{5.4}$$

Calculating the uncertainty in SMF $\phi_i(M_*)$, represented by $\Delta\phi_i(M_*)$, due to N_i^g by propagating the error:

$$\Delta\phi_i(M_*) = \frac{\delta\phi_i(M_*)}{\delta N_i^g} \times \sigma_N \tag{5.5}$$

$$\Delta\phi_i(M_*) = \frac{1}{\Delta \log M_*} \left\langle \frac{1}{V_{\max,j}} \right\rangle \times \sqrt{N_i^g} \tag{5.6}$$

Substituting equation 5.3 in equation 5.6 we get:

$$\Delta\phi_i(M_*) = \frac{1}{\Delta \log M_*} \times \frac{1}{N_i^g} \sum_j \frac{1}{V_{\max,j}} \times \sqrt{N_i^g} \tag{5.7}$$

$$\Delta\phi_i(M_*) = \frac{1}{\sqrt{N_i^g} \times \Delta \log M_*} \times \sum_j \frac{1}{V_{\max,j}} \tag{5.8}$$

Equation 5.8 shows the calculated Poisson uncertainty in the stellar mass function $\phi_i(M_*)$ of KV450 galaxies.

Our results of KV450 galaxy SMF with $1/V_{\max}$ within redshift bins are consistent with the one calculated by Wright et al. (2019) [35]

5.2 SMF for Cluster Galaxies

We analyzed the clusters up to the cluster-centric radius $5R_{500}$, out of 541 eFEDS clusters, there are a total of 313 clusters who has the coverage within $5R_{500}$ shown in Figure 3.2. First, we divide these clusters into two redshift bins (0.385, 0.5) and (0.5, 0.8), where 0.5 is the median redshift within (0.385, 0.8). For the cluster data, we excluded all the clusters below the redshift range 0.385 as the galaxy SMF below $z = 0.3$ had a significant deviation from the galaxy SMF model given in Wright et al. (2018) [34] which shows the survey bias against selecting galaxies having largest angular size [35]. The maximum value of Δz in cluster redshift bin (0.3, 0.4) is approximately 0.085 so while creating the cluster galaxy sample within this range to ensure that the clusters should not contain any galaxy below $z = 0.3$ we set lower cluster redshift limit at 0.385 for the SMF analysis losing the maximum number of low mass clusters. And with the upper redshift limits of the clusters, we started to lose some features in SMF at low masses since we are only left with the most massive galaxies due to the high stellar mass completeness limit at higher redshifts. so we truncated the upper limit at 0.8, losing the clusters at higher redshifts. The total number of clusters used in the analysis is reduced to 105 with the

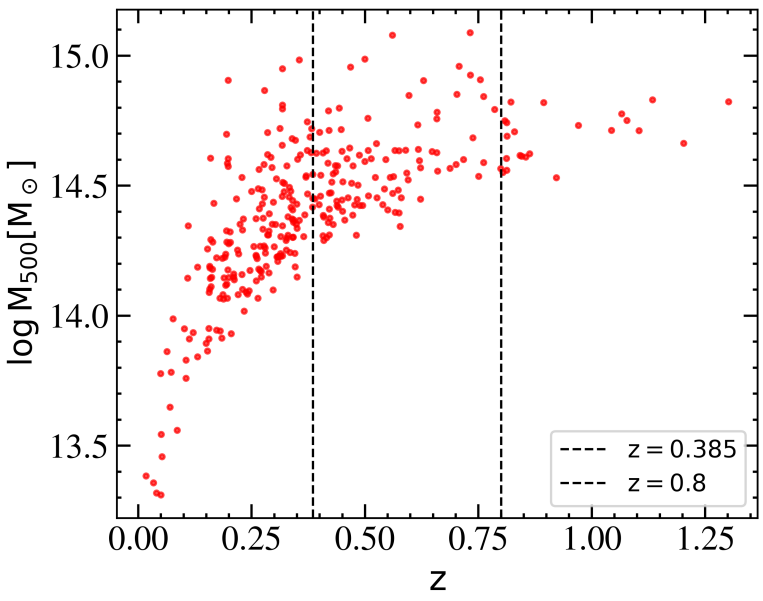


Figure 5.2: The distribution for the total mass of 313 eFEDS clusters (red filled circles) as a function of their redshifts. The final sample of 105 eFEDS clusters used for SMF analysis lies between z = (0.385, 0.8), shown by the dashed vertical lines.

median redshift at 0.5 and median total mass at $10^{14.55} M_{\odot}$, Figure 5.2 shows the total mass vs redshift distribution of the final cluster data used in the analysis.

For calculating the SMF of cluster galaxies, we started by calculating the number of galaxies within the given radial bin of all the clusters, excluding all the galaxies below the mass completeness limit at the highest redshift in the given redshift bin. Then started counting galaxies within stellar mass bins with a bin width of 0.25 dex and then divided by summing all the cluster-centric radial bin volumes of clusters from the final cluster data, which has galaxy coverage within the given radial bin. The cluster galaxy SMF within the i^{th} cluster-centric radial bin is:

$$\phi_i(M_*) = \frac{1}{\Delta \log M_*} \times \frac{N_i^g}{\sum_j V_{j,i}^c} \tag{5.9}$$

now, calculating the Poisson uncertainty in SMF $\phi_i(M_*)$, represented by $\Delta\phi_i(M_*)$, due to N_i^g by propagating the error,

$$\Delta\phi_i(M_*) = \frac{\delta\phi_i(M_*)}{\delta N_i^g} \times \sigma_N$$

Therefore, the uncertainty in the stellar mass function of galaxies becomes,

$$\Delta\phi_i(M_*) = \frac{1}{\Delta \log M_*} \times \frac{\sqrt{N_i^g}}{\sum_j V_{j,i}^c} \tag{5.10}$$

Equation 5.10 shows the calculated Poisson uncertainty in the cluster galaxy SMF.

5.2.1 Background/Foreground Subtraction

After calculating the SMF in different radial bins, we perform a background/foreground subtraction. We used photometric redshift uncertainty Δz to assign galaxies to the host cluster, as a result of which we also include background and foreground galaxies with large redshift uncertainties that are not part of the cluster. To overcome this, we perform background/foreground subtraction by utilizing galaxies in the cluster-centric radial range $4R_{500} - 5R_{500}$ considering the field, as it is far from the clusters and we also masked all the clusters up to $2R_{500}$ which are having coverage within G9 patch shown in Figure 5.3, to ensure that there is no influence of the cluster galaxies on this field SMFs, we subtracted this clusters' coeval field SMF from the earlier calculated cluster galaxy SMFs of the the inner radial bins to get the final cluster galaxy SMF shown in Figure 5.4. Note that we calculate the background field SMFs using only those cluster outskirts for which the cluster galaxy SMF is calculated, while dividing the clusters based on their redshifts, masses, etc.

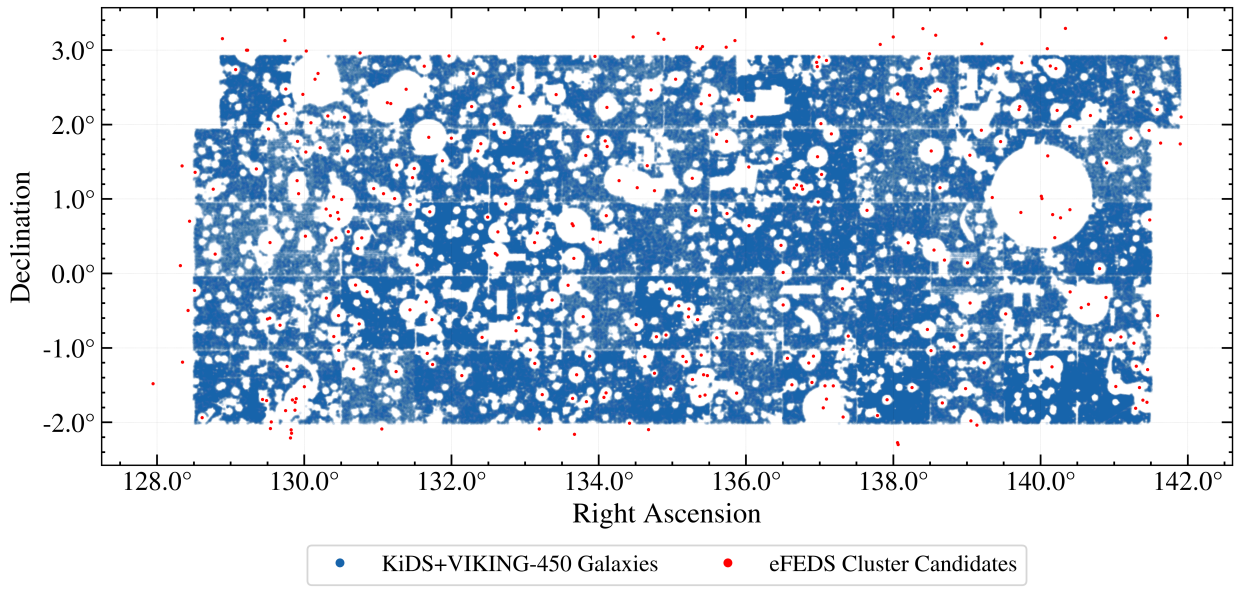
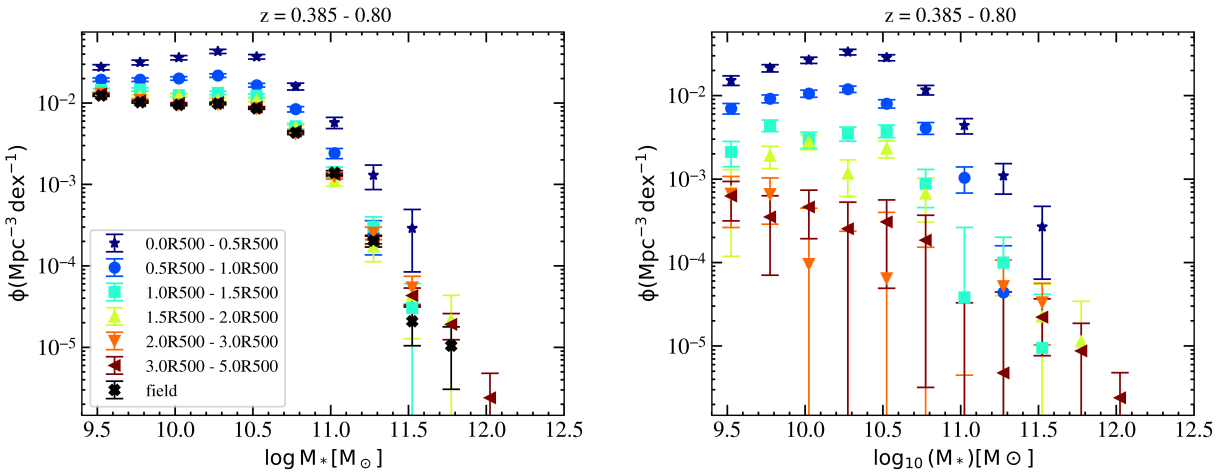


Figure 5.3: Footprint of G9 patch after masking the galaxies within the cluster radius $2R500$. The blue-colored region shows (G9) patch galaxies, and cluster positions are shown with red field circles. Only those clusters are shown in the image that have the coverage within $5R_{500}$.

Figure 5.4 shows the decrease in galaxy density as we move away from the cluster centre. We see a clear decrease in SMFs in radial bins, and a clear detection of SMF out to $2R_{500}$, after which the cluster SMF is mostly consistent with the background level.



(a) (b)

Figure 5.4: Fig. 5.4(a) shows the cluster galaxy SMF within the 6 cluster-centric radial bins before the background subtraction and also shows their coeval field SMF between $4 - 5R500$ with black markers. Fig. 5.4(b) shows the final SMFs after the background/foreground subtraction. For the entire cluster sample within the redshift bin (0.385, 0.8).

Chapter 6

Results and Discussions

Above, we calculated the cluster galaxy SMF for the entire dataset. To quantify the effect of cluster environment on the SMF of cluster galaxies, we further divide the cluster on the basis of their redshift, mass, luminosity, and their ellipticities. We used a fixed bin width for stellar masses equal to 0.25 dex for all of these comparisons. For calculating the cosmological parameters in this work we used ΛCDM cosmology where $\Omega_{\rm m} = 0.3$, $\Omega_\Lambda = 0.7$, $\Omega_{\rm b} = 0.022/h_0^2$, $\sigma_8 = 0.8$, $n_s = 0.96$, and $H_0 = 70\,{\rm km\ s^{-1}\,Mpc^{-1}}$.

For the cluster galaxy sample, we used the common sky coverage area of eFEDS and KV450 we calculated the number of galaxies that should be part of the cluster by calculating cluster radius R_{500} and a redshift range $z \pm \Delta z$ We have also calculated the cluster volume only considering the regions where galaxies are present from the created HEALPix KV450 galaxy map. We have calculated the SMF for cluster galaxies, compared the SMF within radial bins at the same redshift ranges, and also compared the SMF in different radial bins at the same redshift range. We compared the SMF of cluster galaxies by dividing the clusters depending on their total mass and luminosity to see the effect of cluster mass and luminosity on the cluster galaxy SMF.

6.1 Redshift Dependence

To know how the redshift affects the galaxy evolution within the clusters, we split the cluster into two redshift intervals (0.385, 0.5) and (0.5, 0.8), where 0.5 is the median redshift of the final cluster sample. The stellar mass completeness limits for $z = 0.5$, $z = 0.8$ are $9.2 \times 10^8 M_\odot$ and $2.7 \times 10^9 M_\odot$ respectively (for the low and high redshift samples). We show this redshift dependence in the left-hand panel of Figure 6.1, which shows the cluster galaxy SMF as a function of redshift for different cluster-centric radial bins.

We find a clear detection of cluster galaxy SMF out to R_{500} for all the stellar mass range considered, and the SMF detection start declining as we move to larger cluster-centric radii upto $2R_{500}$ after that there is no detection (data points are consistent with background levels). The SMF peaks around $M_* \approx 1 - 2 \times 10^{10} M_\odot$, a feature that is particularly prominent in the innermost radial bin $0 - 0.5R_{500}$, then the SMF starts to flatten in larger radial bins. We see a clear decline in the SMF below masses $M_* < 10^{10} M_\odot$ at $< 0.5R_{500}$ for higher redshift bin, which highlights that the low-mass galaxies have low abundances near cluster centers, likely as such galaxies have low survival as they travel towards the cluster centers. We only find any differences in the SMF as a function of

redshift in the innermost bin, at low stellar masses ($M_* < 10^{10} M_\odot$). The SMF of lower mass galaxies is higher at lower redshift.

6.2 Cluster mass and luminosity dependence

The X-ray luminosity of a galaxy cluster is a well-studied tracer of the cluster's total mass, and the two show a tight scaling relation often used in cosmological studies to calculate one quantity using the other. The mass-luminosity scaling relation for eFEDS clusters is shown in equation 3.1 [6]. In this section, we divide the SMF of cluster galaxies into luminosity ($L^{\rm bol}_{500\,\rm kpc}$) and halo mass ($M_{500}$) bins to study their impact on the stellar properties. The bolometric luminosity is the amount of energy a source emits in unit time across all wavelengths. The luminosity used here is the bolometric luminosity in the band (0.01-100) keV within the 500 kpc radius of the cluster. We used 96 clusters for which the luminosities were defined by Liu et al. (2022)[21] for luminosity-dependent SMF calculations, and all 105 clusters are used for mass-dependent SMF. Since the luminosity and halo mass are correlated with each other by a power law, we see similar trends in the SMF, and the aim here is to identify which quantity shows a clearer impact on the SMF. We divide the clusters with respect to their median mass and luminosity of the sample, which are $10^{14.55} M_\odot$ and 10^{44}erg/s, respectively. The luminosity and mass dependence of the SMF are shown in the middle (2^{nd}) and right-hand (3^{rd}) panels of Figure 6.1, respectively.

We find a slightly clearer impact (though minor to draw any strong conclusions) of luminosity compared to the halo mass on the SMF in the radial bin $0.5R_{500}$, after that the both SMFs for high and low luminosity clusters are mostly consistent in all other radial bins. The SMF of high mass/luminosity clusters shows a peak around $M_* \approx 2 \times 10^{10} M_\odot$, whereas the SMF flattens at low stellar masses for the low mass/luminosity clusters in the innermost radial bin, while the SMF of field galaxies continues to increase at lower stellar masses shown in Figure 6.2[24]. These results support that the SMF of low stellar mass galaxies is sensitive to their environment and that the abundances of these galaxies decline in overdense environments such as galaxy clusters, showing the galaxies grow over time as they reach the cluster centre.

We further divide the median luminosity dependent cluster sample into two redshift bins (a total of four bins) to disentangle the effect of redshift and cluster mass/luminosity on the SMF. In this data sample, there are more high mass or high luminosity clusters in the redshift range (0.5,0.8), approximately twice as many as the low mass clusters. In contrast, for the redshift range (0.385,0.5), there are more low-mass and less-luminous clusters, approximately 1.7 times the high-mass clusters. In Figure 6.2, we show only the results for the innermost radial bin ($0 - 0.5R_{500}$), where we find the most interesting trends. Additionally, we show the background levels, which can be treated as the coeval field levels(field within $4-5R_{500}$) around the cluster sub-samples. The number of clusters used to calculate the coeval fields are same as the clusters used in the SMF analysis for the particular case. We clearly find the difference in the shape of the SMF between the high luminosity/high mass galaxy clusters and the coeval fields. The SMF for low luminosity clusters is flattened in both the redshift bins, while the cluster SMF shows a peak around $M_* \approx 2 \times 10^{10} M_\odot$ compared to the field SMF, which continues to increase at

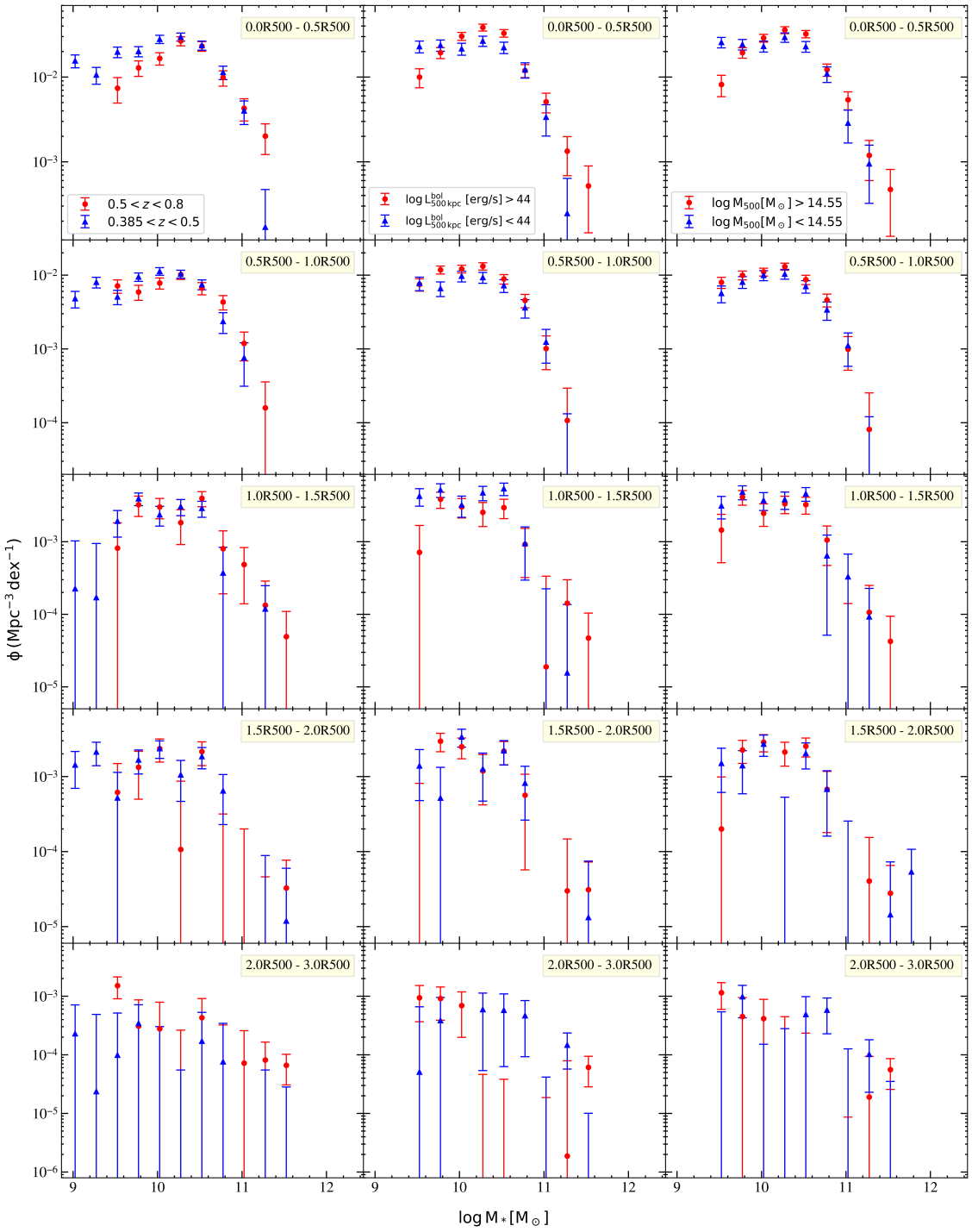


Figure 6.1: Left-hand panel: The comparison of the SMF of cluster galaxies in the redshift bins (0.385, 0.5) and (0.5, 0.8) for six cluster-centric radial bins. **Middle panel:** The SMF comparison for the cluster luminosity bins $(10^{43.65}, 10^{44})$ erg s^{-1} and $(10^{44}, 10^{45.1})$ erg s^{-1} for the entire redshift range (0.385, 0.8). **Right-hand panel:** The SMF comparison for the cluster mass bins $(10^{14.27}, 10^{14.55})$ $M_\odot$ and $(10^{14.55}, 10^{15.08})$ $M_\odot$ for the entire redshift range (0.385, 0.8).

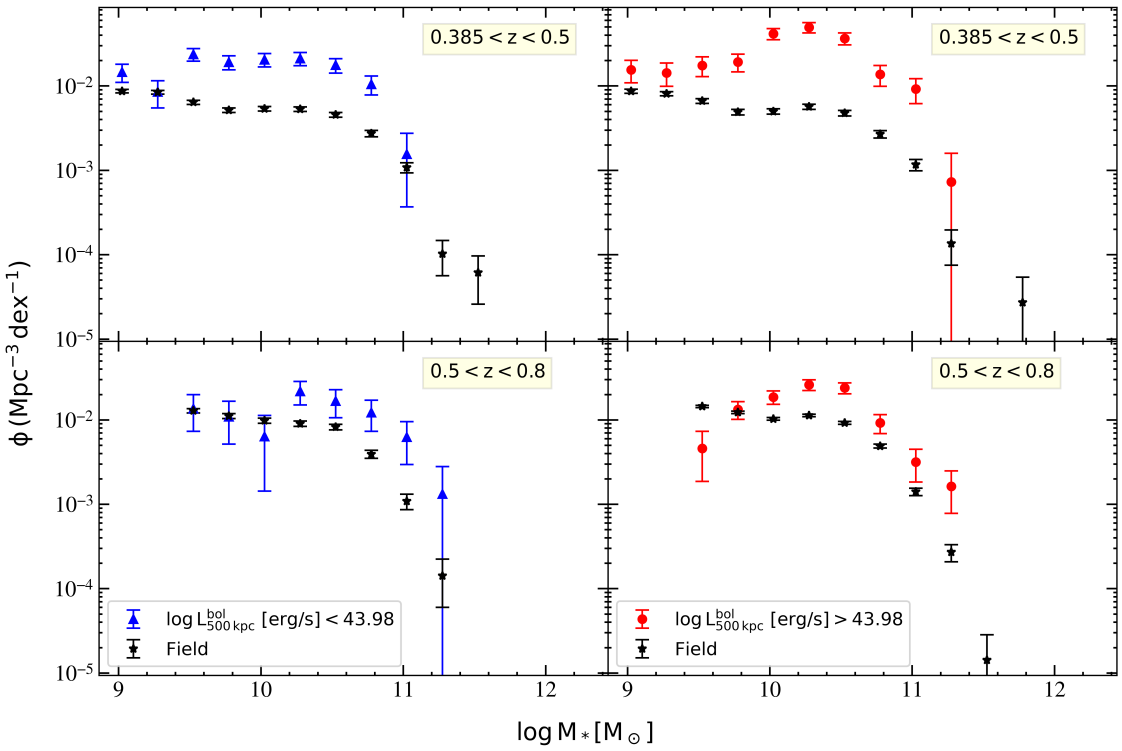


Figure 6.2: The comparison between the luminosity and redshift-dependent SMF of cluster galaxies within $0.5R_{500}$ of the cluster-centric radii and the coeval field galaxy SMF calculated within the cluster-centric radial bin $4-5R_{500}$. The top and the bottom panels correspond to low (0.385, 0.5) and high (0.5, 0.8) redshift bins, respectively. The blue triangles and red circles correspond to low ($\log L^{\rm bol}_{500\,\rm kpc}[\rm erg\,s^{-1}] < 44$) and high ($\log L^{\rm bol}_{500\,\rm kpc}[\rm erg\,s^{-1}] > 44$) luminosity bins, respectively, for both redshift bins. The coeval field galaxy SMF is shown by black stars in all the panels.

lower stellar masses. These results further highlight that the mass/luminosity dependence of the SMF is not due to any hidden redshift dependence, and it persists at both redshift bins considered here. We qualitatively compare our results with Van de Burg et al. (2019)[31], which is closest to the redshift ($z \sim 0.5-0.7$), and the cluster mass ($M_{500} \sim 3\times10^{14}-10^{15}M_\odot$) ranges to our final eFEDS cluster sample. In their Figure 4, they show the radial dependence of the cluster galaxy SMF out to $2R_{500}$. They do not find any significant radial dependence, though there is a minor decline in the total SMF (dominated by the SMF of quiescent galaxies) in the innermost radial bin at $M_* < 2\times10^{10}M_\odot$ (also seen in Van der Burg et al.(2013)[30]. We find a stronger decline in the SMF, especially after dividing the sample into separate mass bins, thus highlighting that this feature is driven by the more massive end of our cluster sample.

6.3 Dynamical State Dependence

The dynamical state of a galaxy cluster is an indicator of the relaxation and merger history of the cluster. The stellar properties of the cluster galaxies are therefore connected to the dynamical state of their host. In this section, we examine the impact of the dynamic state of eFEDS clusters on the SMF of cluster galaxies. We use the ellipticity(e) of the cluster as a proxy for the dynamical state of the cluster, where a lower ellipticity refers

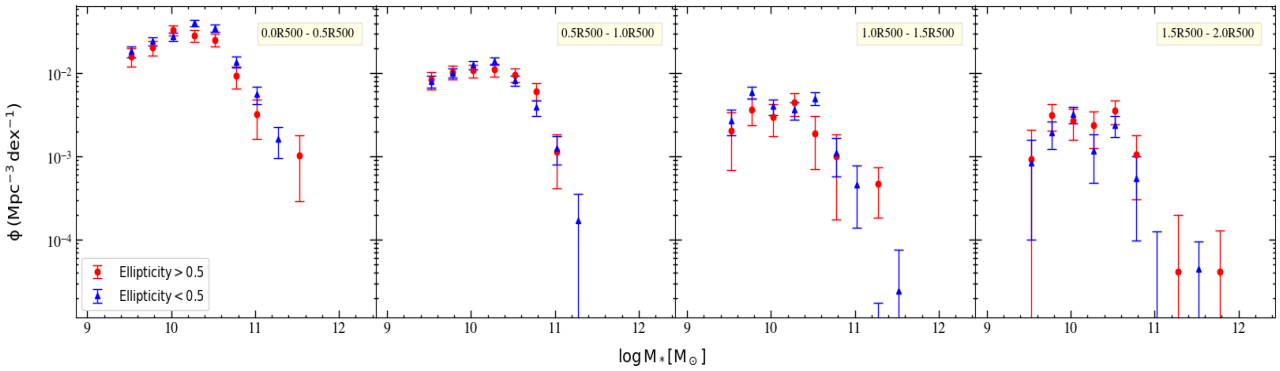


Figure 6.3: The comparison of SMF of cluster galaxies based on the ellipticities of galaxy clusters within the radial bins up to $2R_{500}$. The red circles correspond to the SMF of 10 clusters with ellipticity(e) $e < 0.5$, and the blue triangles correspond to the SMF of clusters with $e > 0.5$ from our final eFEDS cluster sample.

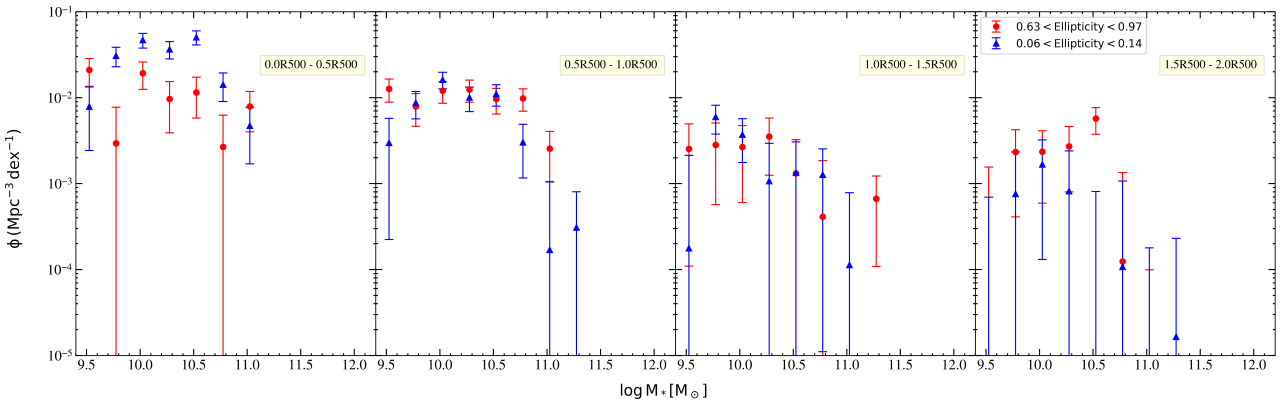


Figure 6.4: The comparison of SMF of cluster galaxies based on the ellipticities of galaxy clusters for the radial bins up to $2R_{500}$. The red circles correspond to the average SMF of 10 clusters with the highest ellipticities, and the blue triangles correspond to the average SMF of 10 clusters with the lowest ellipticities from our final eFEDS cluster sample.

to a more spherical, more relaxed or stable cluster, and a higher ellipticity means an elongated, dynamically disturbed or chaotic cluster[12] [22].

We first started with dividing the cluster sample with respect to their ellipticities and calculated the SMF for the cluster sample with $e < 0.5$ and $e > 0.5$ shown in Figure 6.3 we don't find any difference in these ellipticity bins the SMFS are always consistent in all the bins. So we used the data of 20 clusters, 10 with the least ellipsities in the range ($0.06 < e < 0.97$) and the 10 clusters with the highest ellipticity ($0.63 < e < 0.97$) from the 105 cluster sample. In Figure 6.4, we show the SMF of cluster galaxies up to the radial bins $2R_{500}$ for ten of the eFEDS clusters with the highest (red circles) and the lowest ellipticities (blue triangles). We found the difference between the high ellipticity and low ellipticity cluster only in the radial bin $0-0.5R_{500}$, we did not find any significant differences in the SMF as a function of ellipticity beyond $0.5R_{500}$, and therefore, we only discuss results for the innermost bin here. Galaxy clusters with low ellipticities have higher SMF compared to clusters with high ellipticities. These results indicate that the dynamic state of the cluster has a direct impact on its stellar population, at least

near the cluster center. Young galaxy clusters tend to be more dynamical and hence elliptical compared to the older ones. The trend seen in Figure 6.4 could be tracing the dynamical age of these clusters with high SMF in older clusters compared to the younger ones. However, a more definitive assertion would require a detailed examination of the dynamical state and age of the cluster, beyond a simplistic ellipticity-based categorization, which falls outside the scope of this study.

Chapter 7

Conclusions and Scope for Future Work

7.1 Conclusions

In this work, we have investigated the impact of galaxy clusters on the stellar content of galaxies by estimating the SMF of cluster galaxies as well as their coeval field as a function of cluster redshift, mass, luminosity, and the cluster-centric radii. To do this, we utilize the galaxy cluster sample of 105 clusters from the eFEDS X-ray survey spanning a redshift range $z \sim 0.385-0.8$ and mass range $M_{500} \sim 10^{14.27}-10^{15.08} M_{\odot}$, after applying appropriate selection criteria. We use the galaxy sample from KV450, i.e., KiDS (optical) and VIKING (IR) survey combination, with an approximate overlap of 46 deg^2 with eFEDS survey after removing survey area contaminated by bright foreground stars and incomplete photometry. The stellar masses and photometric redshifts of galaxies are provided by Wright et al. (2019)[35], where we use photometric redshift uncertainties of galaxies to select cluster members, We calculated the number of galaxies that should be part of the cluster by determining the cluster radius R_{500} and selecting galaxies within a redshift range $z \pm \Delta z$. We also calculated the cluster volume by only considering the regions after applying the selection criteria, with the help of the HEALPix KV450 galaxy map we created.

We construct radially-binned cluster galaxy SMFs out to $4R_{500}$, and then divide the cluster sample into mass, redshift, and luminosity bins to further understand the impact of cluster properties on galactic evolution. The main findings of this work are summarized as follows.

- The SMF of the cluster galaxies is detected out to $2R_{500}$. It decreases as we move away from the center of the cluster, and it is consistent with the background level beyond $2R_{500}$ for all the cluster galaxy SMF irrespective of any dependency on redshift, mass, etc.

- We divide the clusters into two redshift bins (0.385,0.5) and (0.5, 0.8) to determine the effect of redshifts on the SMF. We see the SMF of lower stellar mass ($M_* < 10^{10} M_{\odot}$) galaxies is slightly higher at lower redshifts at $r < 0.5R_{500}$ beyond which we do not find any redshift-dependent trends.

- We analyzed the cluster galaxy SMF by dividing the cluster sample based on the median cluster mass, which is at $10^{14.55} M_{\odot}$ and the median bolometric luminosity

at 10^{44}erg/s. The SMF shows a clear peak in the innermost radial bin $(0-0.5R_{500})$ around $M_* \approx 1-2\times10^{10}M_\odot$. This feature is in contrast to the SMF of field galaxies, which continues to increase at lower masses. On further dissecting the cluster sample, we find that this trend is driven by the massive (and hence luminous) galaxy clusters, indicating that the survival rate of low mass galaxies decreases with increasing cluster mass and decreasing Radial distance from the center of the cluster.

- We used the 10 lowest ellipticity clusters and the 10 highest ellipticity clusters to determine the effect of the dynamical nature of the cluster galaxy SMF. We found that the SMF of the highest ellipticity clusters is lower than the SMF of the lowest ellipticity clusters only within $0.5R_{500}$. These results point towards a link between the dynamical age of the clusters and the buildup of stellar content of their galaxies.

We are only able to do this thanks to the large cluster sample from the eFEDS survey with continuous photometric coverage from the KiDS and VIKING surveys.

7.2 Scope for future work

Our results highlight the influence of dense cluster environment, especially near the inner cluster region, on the buildup of the overall stellar mass of cluster galaxies. These results also highlight that it is the lower mass end of the SMF in most massive clusters that is affected significantly (showing the decline in SMF at lower stellar masses). To further dissect the physical processes responsible for these trends, it would be important to classify galaxies into various categories, such as the star-forming and quiescent galaxies, and see how much of the galaxy population in the cluster is quenched and at what distances from the cluster centre in future studies. To know more about the inside processes of galaxy clusters, A comparison with large hydrodynamical simulations with a statistically significant cluster population, such as IllustrisTNG, SIMBA, EAGLE, etc., could also provide more insights into the underlying physical processes affecting the cluster galaxy population.

Bibliography

[1] Healpix. http://healpix.sourceforge.net. Last Edited on 2019-12-19 15:13 UTC.

[2] T. M. C. Abbott, F. B. Abdalla, et al. The dark energy survey: Data release 1. *The Astrophysical Journal Supplement Series*, 239(2):18, nov 2018.

[3] Joshua E. Barnes and Lars Hernquist. Dynamics of interacting galaxies. , 30:705–742, January 1992.

[4] Alberto D. Bolatto, Steven R. Warren, Adam K. Leroy, Fabian Walter, Sylvain Veilleux, Eve C. Ostriker, Jürgen Ott, Martin Zwaan, David B. Fisher, Axel Weiss, Erik Rosolowsky, and Jacqueline Hodge. Suppression of star formation in the galaxy ngc 253 by a starburst-driven molecular wind. *Nature*, 499(7459):450–453, 2013.

[5] Gabriel B Brammer, Pieter G Van Dokkum, and Paolo Coppi. Eazy: a fast, public photometric redshift code. *The Astrophysical Journal*, 686(2):1503, 2008.

[6] Esra Bulbul, I-Non Chiu, Joseph J. Mohr, Michael McDonald, Bradford Benson, Mark W. Bautz, Matthew Bayliss, Lindsey Bleem, Mark Brodwin, Sebastian Bocquet, et al. X-ray properties of spt-selected galaxy clusters at 0.2 lt; z lt; 1.5 observed with xmm-newton. *The Astrophysical Journal*, 871(1):50, jan 2019.

[7] Bulbul, E., Liu, A., Kluge, M., Zhang, X., Sanders, J. S., Bahar, Y. E., Ghirardini, V., Artis, E., Seppi, R., Garrel, C., Ramos-Ceja, M. E., Comparat, J., Balzer, F., Böckmann, K., Brüggen, M., Clerc, N., Dennerl, K., Dolag, K., Freyberg, M., Grandis, S., Gruen, D., Kleinebreil, F., Krippendorf, S., Lamer, G., Merloni, A., Migkas, K., Nandra, K., Pacaud, F., Predehl, P., Reiprich, T. H., Schrabback, T., Veronica, A., Weller, J., and Zelmer, S. The srg/erosita all-sky survey - the first catalog of galaxy clusters and groups in the western galactic hemisphere. *AA*, 685:A106, 2024.

[8] Gene Byrd and Mauri Valtonen. Tidal Generation of Active Spirals and S0 Galaxies by Rich Clusters. , 350:89, February 1990.

[9] S. P. Driver, D. T. Hill, L. S. Kelvin, A. S. G. Robotham, J. Liske, P. Norberg, I. K. Baldry, S. P. Bamford, A. M. Hopkins, J. Loveday, J. A. Peacock, E. Andrae, J. Bland-Hawthorn, S. Brough, et al. Galaxy and Mass Assembly (GAMA): survey diagnostics and core data release. , 413(2):971–995, May 2011.

[10] A. Edge, W. Sutherland, K. Kuijken, S. Driver, R. McMahon, S. Eales, and J. P. Emerson. The VISTA Kilo-degree Infrared Galaxy (VIKING) Survey: Bridging the Gap between Low and High Redshift. *The Messenger*, 154:32–34, December 2013.

[11] K. M. Górski, E. Hivon, A. J. Banday, B. D. Wandelt, F. K. Hansen, M. Reinecke, and M. Bartelmann. HEALPix: A Framework for High-Resolution Discretization and Fast Analysis of Data Distributed on the Sphere. , 622:759–771, April 2005.

[12] C. Gouin, T. Bonnaire, and N. Aghanim. Shape and connectivity of groups and clusters: Effect of the dynamical state and accretion history. , 651:A56, July 2021.

[13] James E. Gunn and III Gott, J. Richard. On the Infall of Matter Into Clusters of Galaxies and Some Effects on Their Evolution. , 176:1, August 1972.

[14] I-Ting Ho (), Anne M. Medling, Joss Bland-Hawthorn, Brent Groves, Lisa J. Kewley, Chiaki Kobayashi, Michael A. Dopita, Sarah K. Leslie, Rob Sharp, James T. Allen, Nathan Bourne, Julia J. Bryant, Luca Cortese, Scott M. Croom, Loretta Dunne, L. M. R. Fogarty, Michael Goodwin, Andy W. Green, Iraklis S. Konstantopoulos, Jon S. Lawrence, Nuria P. F. Lorente, Matt S. Owers, Samuel Richards, Sarah M. Sweet, Edoardo Tescari, and Elisabetta Valiante. The sami galaxy survey: extraplanar gas, galactic winds and their association with star formation history. *Monthly Notices of the Royal Astronomical Society*, 457(2):1257–1278, February 2016.

[15] Yara L. Jaffé, Rory Smith, Graeme N. Candlish, Bianca M. Poggianti, Yun-Kyeong Sheen, and Marc A. W. Verheijen. BUDHIES II: a phase-space view of H I gas stripping and star formation quenching in cluster galaxies. , 448(2):1715–1728, April 2015.

[16] Keunho J. Kim, Matthew B. Bayliss, Allison G. Noble, Gourav Khullar, Ethan Cronk, Joshua Roberson, Behzad Ansarinejad, Lindsey E. Bleem, Benjamin Floyd, Sebastian Grandis, Guillaume Mahler, Michael A. McDonald, Christian L. Reichardt, Alexandro Saro, Keren Sharon, Taweewat Somboonpanyakul, and Veronica Strazzullo. A gradual decline of star formation since cluster infall: New kinematic insights into environmental quenching at 0.3 lt; z lt; 1.1. *The Astrophysical Journal*, 955(1):32, sep 2023.

[17] M. G. Kitzbichler and S. D. M. White. A calibration of the relation between the abundance of close galaxy pairs and the rate of galaxy mergers. , 391(4):1489–1498, December 2008.

[18] M. Klein, M. Oguri, J. J. Mohr, S. Grandis, V. Ghirardini, T. Liu, A. Liu, E. Bulbul, J. Wolf, J. Comparat, M. E. Ramos-Ceja, J. Buchner, I. Chiu, N. Clerc, A. Merloni, H. Miyatake, S. Miyazaki, N. Okabe, N. Ota, F. Pacaud, M. Salvato, and S. P. Driver. The eROSITA Final Equatorial-Depth Survey (eFEDS). Optical confirmation, redshifts, and properties of the cluster and group catalog. , 661:A4, May 2022.

[19] Mariska Kriek, Pieter G. van Dokkum, Ivo Labbé, Marijn Franx, Garth D. Illingworth, Danilo Marchesini, and Ryan F. Quadri. An Ultra-Deep Near-Infrared Spectrum of a Compact Quiescent Galaxy at z = 2.2. , 700(1):221–231, July 2009.

[20] Konrad Kuijken, Catherine Heymans, Hendrik Hildebrandt, Reiko Nakajima, Thomas Erben, Jelte T. A. de Jong, Massimo Viola, Ami Choi, Henk Hoekstra, Lance Miller, Edo van Uitert, Alexandra Amon, Chris Blake, Margot Brouwer, Axel

Buddendiek, Ian Fenech Conti, Martin Eriksen, Aniello Grado, Joachim Harnois-Déraps, Ewout Helmich, Ricardo Herbonnet, Nancy Irisarri, Thomas Kitching, Dominik Klaes, Francesco La Barbera, Nicola Napolitano, Mario Radovich, Peter Schneider, Cristóbal Sifón, Gert Sikkema, Patrick Simon, Alexandru Tudorica, Edwin Valentijn, Gijs Verdoes Kleijn, and Ludovic van Waerbeke. Gravitational lensing analysis of the Kilo-Degree Survey. , 454(4):3500–3532, December 2015.

[21] A. Liu, E. Bulbul, V. Ghirardini, T. Liu, M. Klein, N. Clerc, Y. Özsoy, M. E. Ramos-Ceja, F. Pacaud, J. Comparat, N. Okabe, Y. E. Bahar, V. Biffi, H. Brunner, M. Brüggen, J. Buchner, J. Ider Chitham, I. Chiu, K. Dolag, E. Gatuzz, J. Gonzalez, D. N. Hoang, G. Lamer, A. Merloni, K. Nandra, M. Oguri, N. Ota, P. Predehl, T. H. Reiprich, M. Salvato, T. Schrabback, J. S. Sanders, R. Seppi, and Q. Thibaud. The eROSITA Final Equatorial-Depth Survey (eFEDS). Catalog of galaxy clusters and groups. , 661:A2, May 2022.

[22] Zhenjie Liu, Jun Zhang, Cong Liu, and Hekun Li. Ellipticities of Galaxy Cluster Halos from Halo–Shear–Shear Correlations. , 979(2):200, February 2025.

[23] D. Merritt. Relaxation and tidal stripping in rich clusters of galaxies. II. Evolution of the luminosity distribution. , 276:26–37, January 1984.

[24] Adam Muzzin, Danilo Marchesini, Mauro Stefanon, Marijn Franx, Henry J. McCracken, Bo Milvang-Jensen, James S. Dunlop, J. P. U. Fynbo, Gabriel Brammer, Ivo Labbé, and Pieter G. van Dokkum. The Evolution of the Stellar Mass Functions of Star-forming and Quiescent Galaxies to z = 4 from the COSMOS/UltraVISTA Survey. , 777(1):18, November 2013.

[25] Adam Muzzin, Danilo Marchesini, Mauro Stefanon, Marijn Franx, Bo Milvang-Jensen, James S. Dunlop, J. P. U. Fynbo, Gabriel Brammer, Ivo Labbé, and Pieter van Dokkum. A public ks-selected catalog in the cosmos/ultravista field: Photometry, photometric redshifts, and stellar population parameters*,†. *The Astrophysical Journal Supplement Series*, 206(1):8, may 2013.

[26] Maarten Schmidt. Space distribution and luminosity functions of quasi-stellar radio sources. *Astrophysical Journal, vol. 151, p. 393*, 151:393, 1968.

[27] Rahul Shetty and Eve C. Ostriker. Cloud and star formation in disk galaxy models with feedback. *The Astrophysical Journal*, 684(2):978–995, September 2008.

[28] M. F. Skrutskie, R. M. Cutri, R. Stiening, M. D. Weinberg, S. Schneider, J. M. Carpenter, C. Beichman, R. Capps, T. Chester, J. Elias, J. Huchra, J. Liebert, C. Lonsdale, D. G. Monet, S. Price, P. Seitzer, T. Jarrett, J. D. Kirkpatrick, J. E. Gizis, E. Howard, T. Evans, J. Fowler, L. Fullmer, R. Hurt, R. Light, E. L. Kopan, K. A. Marsh, H. L. McCallon, R. Tam, S. Van Dyk, and S. Wheelock. The two micron all sky survey (2mass). *The Astronomical Journal*, 131(2):1163, feb 2006.

[29] Adam R. Tomczak, Brian C. Lemaux, Lori M. Lubin, Roy R. Gal, Po-Feng Wu, Bradford Holden, Dale D. Kocevski, Simona Mei, Debora Pelliccia, Nicholas Rumbaugh, and Lu Shen. Glimpsing the imprint of local environment on the galaxy stellar mass function. , 472(3):3512–3531, December 2017.

[30] R. F. J. van der Burg, A. Muzzin, H. Hoekstra, C. Lidman, A. Rettura, G. Wilson, H. K. C. Yee, H. Hildebrandt, D. Marchesini, M. Stefanon, R. Demarco, and K. Kuijken. The environmental dependence of the stellar mass function at z ~1. Comparing cluster and field between the GCLASS and UltraVISTA surveys. , 557:A15, September 2013.

[31] Remco FJ van der Burg, Sean McGee, Hervé Aussel, Håkon Dahle, Monique Arnaud, Gabriel W Pratt, and Adam Muzzin. The stellar mass function of galaxies in planck-selected clusters at 0.5¡ z¡ 0.7: new constraints on the timescale and location of satellite quenching. *Astronomy & Astrophysics*, 618:A140, 2018.

[32] M. Völschow, R. Banerjee, and B. Körtgen. Star formation in evolving molecular clouds. *Astronomy amp; Astrophysics*, 605:A97, September 2017.

[33] JR Weaver, I Davidzon, S Toft, O Ilbert, HJ McCracken, KML Gould, CK Jespersen, C Steinhardt, CDP Lagos, PL Capak, et al. Cosmos2020: The galaxy stellar mass function-the assembly and star formation cessation of galaxies at 0.2¡ z 7.5. *Astronomy & Astrophysics*, 677:A184, 2023.

[34] A. H. Wright, S. P. Driver, and A. S. G. Robotham. GAMA/G10-COSMOS/3D-HST: Evolution of the galaxy stellar mass function over 12.5 Gyr. , 480(3):3491–3502, November 2018.

[35] Angus H. Wright, Hendrik Hildebrandt, Konrad Kuijken, Thomas Erben, Robert Blake, Hugo Buddelmeijer, Ami Choi, Nicholas Cross, Jelte T. A. de Jong, Alastair Edge, Carlos Gonzalez-Fernandez, Eduardo González Solares, Aniello Grado, Catherine Heymans, Mike Irwin, Aybuke Kupcu Yoldas, James R. Lewis, Robert G. Mann, Nicola Napolitano, Mario Radovich, Peter Schneider, Cristóbal Sifón, William Sutherland, Eckhard Sutorius, and Gijs A. Verdoes Kleijn. KiDS+VIKING-450: A new combined optical and near-infrared dataset for cosmology and astrophysics. , 632:A34, December 2019.

[36] Angus H. Wright, Konrad Kuijken, Hendrik Hildebrandt, Mario Radovich, Maciej Bilicki, Andrej Dvornik, and 0thers. The fifth data release of the Kilo Degree Survey: Multi-epoch optical/NIR imaging covering wide and legacy-calibration fields. , 686:A170, June 2024.

[37] Andrea Zonca, Leo Singer, Daniel Lenz, Martin Reinecke, Cyrille Rosset, Eric Hivon, and Krzysztof Gorski. healpy: equal area pixelization and spherical harmonics transforms for data on the sphere in python. *Journal of Open Source Software*, 4(35):1298, March 2019.